Available online at www.sciencedirect.com
SCIENCE DIRECT®
ELSEVIER
Nuclear Instruments and Methods in Physics Research A 520 (2004) 281–284
NUCLEAR INSTRUMENTS & METHODS IN PHYSICS RESEARCH Section A
www.elsevier.com/locate/nima

Characterization and modeling of transition edge sensors for high resolution X-ray calorimeter arrays

T. Saab[a,*], E. Apodacas[a,b], S.R. Bandler[a,c], K. Boyce[a], J. Chervenak[a], E. Figueroa-Feliciano[a], F. Finkbeiner[a,d], C. Hammock[a,d], R. Kelley[a], M. Lindeman[a,c], F.S. Porter[a], C.K. Stahle[a]

[a] *NASA Goddard Space Flight Center, Greenbelt, MD 20771, USA*
[b] *QSS Group, Lanham, MD 20706, USA*
[c] *University of Maryland, College Park, MD 20742, USA*
[d] *Science Systems and Applications, Lanham, MD 20706, USA*

Abstract

Characterizing and understanding, in detail, the behavior of a Transition Edge Sensor (TES) is required for achieving an energy resolution of 2 eV at 6 keV desired for future X-ray observatory missions. This paper will report on a suite of measurements (e.g. impedance and I–V among others) and simulations that were developed to extract a comprehensive set of TES parameters such as heat capacity, thermal conductivity, and $R(T,I)$, $\alpha(T,I)$, and $\beta_I(T,I)$ surfaces. These parameters allow for the study of the TES calorimeter behavior at and beyond the small signal regime.

PACS: 85.25.Am; 63.20.Kr; 95.55.Ka

Keywords: Transition edge sensor; Electrical and thermal model; Device characterization

1. Introduction

The behavior of a Transition Edge Sensor (TES) in the small signal, linear regime is described by two differential equations [1] where the two free parameters, $\alpha = \partial \ln R/\partial \ln T$, and $\beta_I = \partial \ln R/\partial \ln I$, are treated as constants. In order to obtain optimal resolution over a large energy range, however, one must make understand the behavior of pulses for which a large portion of the transition is sampled. For such a case α, and β_I cease to be constants and must be treated as functions of temperature and current. Knowledge of the function $R(T,I)$ of a TES, along with various heat capacities and thermal conductivities allows for the construction of a comprehensive, non-linear model of the TES response to absorbed X-rays.

2. Mapping the R(T,I) surface

The I–V curves of a TES illustrate a DC response and thus are a good way of extracting $R(T,I)$ information independently of other

*Corresponding author.
E-mail address: tsaab@milkyway.gsfc.nasa.gov (T. Saab).

0168-9002/$ - see front matter
doi:10.1016/j.nima.2003.11.238

quantities such as C, G, or the inductance of the circuit (L). Since our TESs are operated in voltage bias mode [1] an I–V curve traces a path on the $R(T,I)$ surface which keeps the power dissipation, not the current, in the TES constant.

Eq. (1) shows the dependence of the TES power dissipation on base temperature (T_b) and thermal conductivity (G_{pb})

$$P = k(T_e^n - T_b^n)$$

$$G_{pb} \equiv \frac{\partial P}{\partial T} = nkT_e^{n-1} \tag{1}$$

where T_e is the TES electron temperature and n is a constant. The I–V measurement allows a direct determination of both G_{pb} and n, by fitting Eq. (1) to the data as shown in Fig. 1.

The dependence of the TES impedance, $Z_{TES}(f)$, on the various TES parameters is given in [2]. In the limit of high and low frequencies the impedance is seen to depend primarily on α and β_i as shown in Eq. (2).

$$Z_{TES}(f \to \infty) = R_0(1 + \beta_i)$$

$$Z_{TES}(f \to 0) = R_0\left[\frac{-I_0^2 R_0 \alpha - G_{pb} T_0(1 + \beta_i)}{I_0^2 R_0 \alpha - G_{pb} T_0}\right] \tag{2}$$

where T_0, I_0, and R_0 are the equilibrium temperature, current, and resistance, respectively, of the TES at a given bias. By measuring the high and low frequency impedance as a function of TES bias voltage we obtain α, and β_i throughout the transition as shown in Fig. 2. This information is complementary to the I–V data and we are able to reconstruct a profile of the $R(T,I)$ surface as shown in Fig. 3.

Knowledge of the $R(T,I)$ surface is not just relevant for properly modeling the TES behavior.

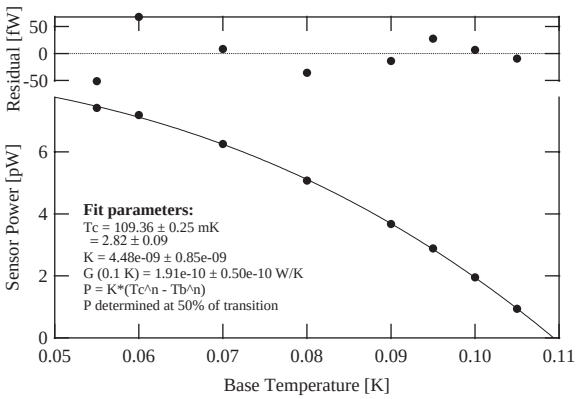

Fig. 1. Power dissipation in the TES as a function of base temperature. Fitting Eq. (1) to this data yields the TES to heat bath thermal conductivity (G_{pb}) and the exponent of the power law (n).

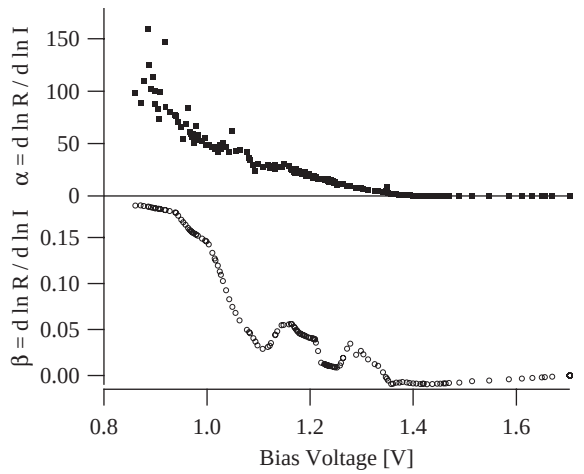

Fig. 2. Variation of α and β_i throughout the transition. This data was obtained in a model independent fashion by measuring the high and low frequency limits of the TES impedance $Z_{TES}(f)$.

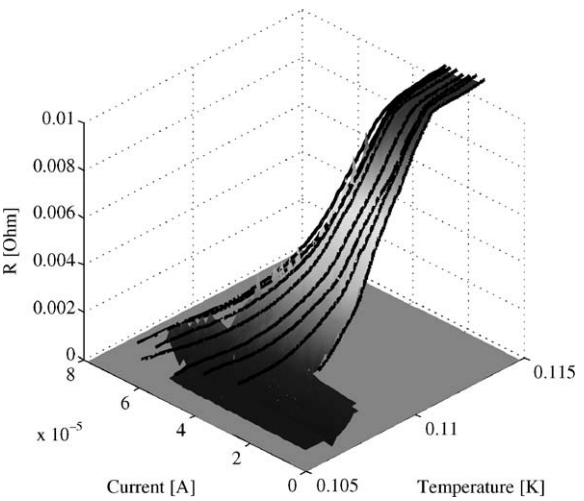

Fig. 3. Reconstructed $R(T,I)$ surface. The shape of the superconducting transition is reconstructed from I–V data and can be used as an input to the TES model.

Kinks in the surface can have significant (usually detrimental) effects on pulse shape and noise response, and we must ensure that the TES is not biased near such a point.

3. Measuring *C* & *G*

All TES properties described so far are model independent and are directly measurable. In order to fully understand the behavior and resolution of the TES beyond the linear, small signal regime a complete TES model is required. Fig. 4 shows a schematic of the TES model in which the TES is coupled to the heat bath via the phonon system, while the X-ray absorber is connected to the TES electron system.

The TES pulse shape, impedance characteristics, and noise spectrum are computed numerically and fitted to data in order to obtain values for the various *C*s and *G*s. Fig. 5 shows impedance data through the transition of an actual and a simulated TES. The parameters used to simulate the impedance are not the result of a fit, but have been chosen to demonstrate a qualitative agreement with the data. Fig. 6 shows a 6 keV X-ray pulse with two decay time constants that is well fitted by our model.

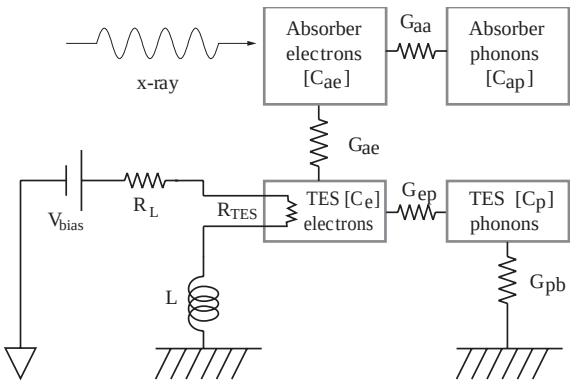

Fig. 4. Electrical and thermal circuit representing the TES calorimeter model. With such a model linear and non-linear simulations of pulse shapes, impedance responses, and *I–V* characteristics can be calculated and compared to data in order to pin down the values of the various conductances (*G*) and heat capacities (*C*).

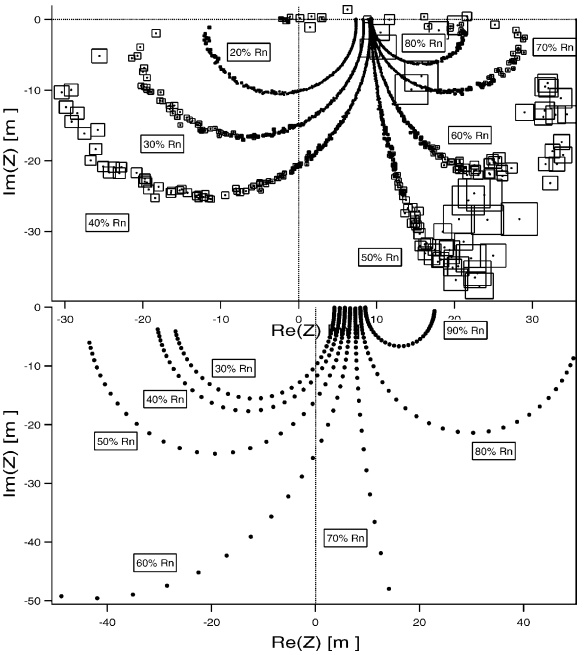

Fig. 5. Variation of TES impedance ($Z_{TES}(f)$) throughout the transition for an actual TES (top panel) and a model simulation (bottom panel). The simulation parameters are not the result of a fit, but are chosen to indicate qualitative agreement.

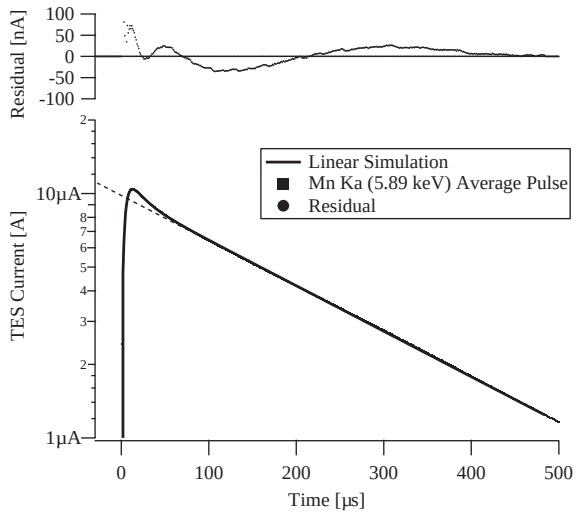

Fig. 6. A 6 keV X-ray pulse exhibiting two decay time constants is well fitted by a TES model which assumes a hanging absorber phonon heat capacity.

References

[1] M.A. Lindeman, et al., Detailed characterization of Mo/Au TES microcalorimeters, in: Low Temperature Detectors, Ninth International Workshop on Low Temperature Detectors, Madison, WI, USA, July 2002, pp. 219–222.

[2] M.A. Lindeman, et al., Impedance measurements and modeling of a test calorimeter, J. Appl. Phys., submitted for publication, 2003.